Mechanisms controlling crescentic bar amplitude

Roland Garnier,[1,2] Nicholas Dodd,[1] Albert Falqués,[3] and Daniel Calvete[3]

Received 2 June 2009; revised 5 November 2009; accepted 17 December 2009; published 15 April 2010.

[1] The formation of crescentic bars from self-organization of an initially straight shore-parallel bar for shore-normal incident waves is simulated with a two-dimensional horizontal morphodynamical model. The aim is to investigate the mechanisms behind the saturation process defined as the transition between the linear regime (maximum and constant growth of the crescentic pattern) and the saturated state (negligible growth). The global properties of the morphodynamical patterns over the whole computational domain are studied ("global analysis"). In particular, consideration of the balance of the potential energy of the emerging bar gives its growth rate from the difference between a production term (related to the positive feedback leading to the instability) and a damping term (from the gravity-driven downslope transport). The production is approximately proportional to the average over the domain of the cross-shore flow velocity times the bed level perturbation. The damping is essential for the onset of the saturation, but it remains constant while the production decreases. Thus, it is notable that the saturation occurs because of a weakening of the instability mechanism rather than an increase of the damping. A reason for the saturation of the crescentic bar growth is the change in bar shape from its initial stage rather than the growth in amplitude itself. This change is mainly characterized by the narrowing of the rip channels, the onshore migration of the crests, and the change in the mean beach profile due to alongshore variability. These properties agree with observations of mature rip channel systems in nature.

Citation: Garnier, R., N. Dodd, A. Falqués, and D. Calvete (2010), Mechanisms controlling crescentic bar amplitude, *J. Geophys. Res.*, *115*, F02007, doi:10.1029/2009JF001407.

1. Introduction

[2] The surf zone of sandy barred beaches is characterized by the presence of one or several shore-parallel bars. They are not always straight in plan view but are often meandering with deep and shallow sections alternating along the bars with a striking regularity. These bars are called crescentic bars (or lunate bars) and are probably the most documented and observed rhythmic features in the surf zone [*Wright and Short*, 1984; *Short*, 1999; *van Enckevort et al.*, 2004; *Lafon et al.*, 2004; *Castelle et al.*, 2007; *Ruessink et al.*, 2007]. They are associated with the typical current circulation of strong jet-like offshore-oriented currents (called rip currents) in the deep sections (called rip channels) and weaker wider onshore currents in the shallow sections.

[3] Understanding the formation and the evolution of crescentic bar systems is an active area of research. Although their formation had been attributed to the hydrodynamical forcing of infragravity edge waves [*Bowen and Inman*, 1971; *Holman and Bowen*, 1982], it is well accepted nowadays that the feedback from the morphology into the flow is the primary cause of their formation [*Deigaard et al.*, 1999; *Falqués et al.*, 2000; *Damgaard et al.*, 2002; *Reniers et al.*, 2004; *Klein and Schuttelaars*, 2006; *van Leeuwen et al.*, 2006; *Calvete et al.*, 2007; *Dronen and Deigaard*, 2007; *Garnier et al.*, 2008; *Smit et al.*, 2008]. Apart from *Dronen and Deigaard* [2007], who used a quasi-three-dimensional area (Q3D) model, all these self-organization studies are based on wave- and depth-averaged process-based (two-dimensional horizontal (2DH)) morphological modeling. They show that crescentic bar systems would emerge from a free instability because of a positive feedback between waves, currents, and morphology.

[4] Under normal or near-normal wave incidence, the positive feedback is explained by the bed surf mechanism [*Falqués et al.*, 2000; *Caballeria et al.*, 2002; *Ribas et al.*, 2003; *Calvete et al.*, 2005; *Garnier et al.*, 2008]. Crescentic bars are sometimes viewed as two adjacent series of shoals and troughs. These series are antisymmetric with respect to a line parallel to the coast. In particular, the bed surf mechanism explains that these crescentic features can appear on an alongshore uniform beach if the depth-averaged sediment concentration profile admits a local maximum. The position of the maximum defines the antisymmetric axis,

[1] Environmental Fluid Mechanics Research Centre, Process and Environmental Division, Faculty of Engineering, University of Nottingham, Nottingham, UK.
[2] Now at Departament de Física Aplicada, Universitat Politécnica de Catalunya, Barcelona, Spain.
[3] Departament de Física Aplicada, Universitat Politécnica de Catalunya, Barcelona, Spain.

0148-0227/10/2009JF001407

which, for a barred beach, is close to the top of the bar. *Garnier et al.* [2008] showed that, for random waves over a barred beach, the inner series (shoreward of the axis) emerges from a free instability but the outer is forced by the inner so that its amplitude is weaker and crescentic bars are mainly defined by the inner series.

[5] Most of these modeling studies, based either on the linear stability analysis or on nonlinear modeling, are limited to the bar formation and to the earliest stage of the bar evolution because of the model formulation (linear models) or because the nonlinear models break down. The reason for this nonlinear model limitation is not clear and has not been investigated. The reason is not necessarily numerical; it could be a lacuna in the physics, casting doubt on whether the saturation of the growth of crescentic bars can be described by numerical models. Recently, *Garnier et al.* [2008] reproduced this saturation by using a simple 2DH model, but the physical mechanisms are still unexplored. They reached the nonlinear regime and were able to simulate the finite amplitude behavior of crescentic bars, showing that the final bar shape differs from the initial one: the channels become narrower than the crests (this is associated with jet-like rip currents), the channels tend to migrate offshore, and the shoals tend to migrate onshore.

[6] Finite amplitude modeling of morphological features is fundamental for any comparison with observations. The saturation of the bed form growth has been obtained for other morphodynamical systems such as shoreface-connected sand ridges [*Calvete and de Swart*, 2003; *Roos et al.*, 2004; *Vis-Star et al.*, 2008], sand ripples [*Marieu et al.*, 2008], and shore-transverse sandbars [*Garnier et al.*, 2006]. A method to investigate the mechanisms of saturation was introduced by *Garnier et al.* [2006] and extended by *Vis-Star et al.* [2008]; it is called the global analysis. It consists of studying the global properties of the bed forms over the whole computational domain by deriving a potential energy balance of the bed forms. For both the shoreface-connected ridges and the transverse bars, the saturation of the bed forms occurs because of the balance between a production and a damping term. However, the reason for this balance has not yet been explained.

[7] The objective of this contribution is to investigate the mechanisms behind the saturation of the growth of crescentic bars from the numerical experiments of *Garnier et al.* [2008] by using the global analysis. It is organized as follows. Section 2 presents the methodology by introducing the equations and the hypothesis necessary to understand the derivation of the global analysis. The general results and the main variables of the analysis are given in section 3. The physical mechanisms are explained in section 4. Section 5 gives the conclusions.

2. Methodology

2.1. Governing Equations

[8] The 2DH MORFO55 model solves the phase-averaged nonlinear shallow water equations with sediment transport and bed updating [*Mei*, 1989; *Caballeria et al.*, 2002; *Garnier et al.*, 2006, 2008]. The water mass (equation (1)), the momentum (equation (2)), and the sediment mass (equation (3)) conservation equations read (repeated indices indicate summation with $i, j = 1, 2$; t is time)

$$\frac{\partial D}{\partial t} + \frac{\partial}{\partial x_j}\left(D\, v_j\right) = 0, \tag{1}$$

$$\frac{\partial v_i}{\partial t} + v_j \frac{\partial v_i}{\partial x_j} = -g\frac{\partial z_s}{\partial x_i} - \frac{1}{\rho D}\frac{\partial}{\partial x_j}\left(S'_{ij} - S''_{ij}\right) - \frac{\tau_{bi}}{\rho D}, \tag{2}$$

$$\frac{\partial z_b}{\partial t} + \frac{\partial q_j}{\partial x_j} = 0, \tag{3}$$

where D is the total mean depth, $\mathbf{v}$ is the depth-averaged mean velocity vector ($\mathbf{v} = (v_1, v_2) = (u, v)$), g is the acceleration due to gravity ($g = 9.8\ \mathrm{m\ s^{-2}}$), z_s is the mean sea level, ρ is the water density ($\rho = 1024\ \mathrm{kg\ m^{-3}}$), S' is the wave radiation stress tensor, S'' is the turbulent Reynolds stress tensor, $\boldsymbol{\tau}_b$ is the bed shear stress vector, z_b is the bed level, and $\mathbf{q}$ is the horizontal sediment flux vector. Note that the bed porosity effect has been included in the sediment flux in order to simplify the notations. The wave field is solved by using the wave energy dissipation equation and Snell's law; the wave current interaction has been removed as it only has a small effect on the presented results. For more details, refer to *Garnier et al.* [2006, 2008].

[9] An initial topography that is strictly alongshore uniform forced by a stationary alongshore uniform wave field is considered. Since the dynamics of crescentic bars are assumed to be mainly governed by rip current circulation, the cross-shore transport driven by undertow, wave nonlinearities, and gravity is disregarded. This means that those contributions are considered to be in balance for this basic state, which is therefore an equilibrium state. When departures from this bathymetry develop, the sediment flux $\mathbf{q}$ does not vanish. It is based on the Soulsby–Van Rijn total load formula [*Soulsby*, 1997] (see *Garnier et al.* [2008] for details) and reads

$$\mathbf{q} = \alpha\left(\mathbf{v} - \gamma\, u_b\, \nabla h\right), \tag{4}$$

where α is the stirring factor, which includes the bed porosity $p = 0.4$ ($\alpha = \alpha_{\mathrm{svr}}/(1-p)$); γ is the bed slope coefficient; u_b is the root-mean-square wave orbital velocity amplitude at the bottom; and h is the bed level deviation from initial equilibrium ($h = z_b - z_b^0$, where z_b^0 is the initial bed level). The stirring factor α_{svr} is computed as follows:

$$\alpha_{\mathrm{svr}} = A_S\left(u_s - u_c\right)^{2.4} \quad \text{if } u_s > u_c$$

$$\alpha_{\mathrm{svr}} = 0 \quad \text{otherwise,}$$

according to *Soulsby* [1997], where A_S and u_c depend essentially on sediment characteristics and water depth [*Soulsby*, 1997]. The stirring velocity u_s reads

$$u_s = \left(|\mathbf{v}|^2 + \frac{0.018}{c_D}\, u_b^2\right)^{1/2},$$

c_D being the morphodynamical drag coefficient [*Soulsby*, 1997]. Essentially, $\alpha\ \mathbf{v}$ describes the contribution from the circulation, and $-\alpha\gamma\ u_b\ \nabla h$ describes the contribution

that would bring the bathymetry back to the equilibrium profile if there were no circulation.

2.2. Bottom Evolution Equation Approximation

[10] The Bottom Evolution Equation (BEE) has been introduced by *Falqués et al.* [2000] as an approximate expression of bed changes to facilitate understanding bed evolution in connection with hydrodynamics. For completeness, we briefly revisit it in our context. By using the sediment transport formula (equation (4)), the sediment conservation equation (equation (3)) reads

$$\frac{\partial h}{\partial t} = -\boldsymbol{\nabla}\cdot(\alpha\mathbf{v}) + \boldsymbol{\nabla}\cdot(\Gamma\boldsymbol{\nabla}h),$$

where $\Gamma = \gamma\ \alpha\ u_b$. According to the water mass conservation equation (equation (1)),

$$\boldsymbol{\nabla}\cdot(\alpha\mathbf{v}) = \boldsymbol{\nabla}\cdot(C\,D\mathbf{v}) = D\mathbf{v}\cdot\boldsymbol{\nabla}C - C\frac{\partial D}{\partial t},$$

where C is the equivalent depth-averaged concentration ($C = \alpha/D$), also called the potential stirring.

[11] From the combination of the two previous equations, and by assuming $|\partial D/\partial t| \simeq |\partial h/\partial t|$ (the flow is assumed to adjust instantaneously to the bed changes), we obtain

$$(1-C)\frac{\partial h}{\partial t} \simeq -D\,\mathbf{v}\cdot\boldsymbol{\nabla}C + \boldsymbol{\nabla}\cdot(\Gamma\boldsymbol{\nabla}h).$$

Finally, by using the approximation $C \ll 1$ (for instance, $C \simeq 0.001$ from *Garnier et al.* [2008]), the BEE reads

$$\frac{\partial h}{\partial t} \simeq -D\,\mathbf{v}\cdot\boldsymbol{\nabla}C + \boldsymbol{\nabla}\cdot(\Gamma\boldsymbol{\nabla}h). \tag{5}$$

2.3. Global Analysis

[12] The global analysis of beach evolution was introduced by *Garnier et al.* [2006] and consists of analyzing variables that are integrated over the computational domain. It differs from the local analysis used by *Garnier et al.* [2008], which can only explain the formation of features and not the saturation of the growth. The limitation of the local analysis can be understood because the bars can still be in movement while their growth on average is already saturated, so that some sort of equilibrium is reached (we refer to this as a "dynamical equilibrium"). For instance, for oblique waves, an equilibrium state is reached, but the bars still migrate; thus, the local analysis still predicts erosion and deposition at some locations. The global analysis for the evolution of transverse bar systems appearing on a planar beach [*Garnier et al.*, 2006] is extended here to the case of rip channels developing from the deformation of an initially alongshore uniform parallel bar obtained by *Garnier et al.* [2008].

[13] We first introduce the overbar notation to define an average over the computational domain. It reads, for any function $f = f(x, y)$,

$$\overline{f} = \frac{1}{L_x L_y}\int_0^{L_y}\int_0^{L_x} f\ \mathrm{d}x\,\mathrm{d}y,$$

where L_x (L_y) is the cross-shore (alongshore) length of the computational domain. Following *Garnier et al.* [2006], the production $\mathcal{P}$ and the damping Δ can be defined by

$$\mathcal{P} = -\overline{h\boldsymbol{\nabla}\cdot(\alpha\mathbf{v})}, \tag{6}$$

$$\Delta = -\overline{h\boldsymbol{\nabla}\cdot(\Gamma\boldsymbol{\nabla}h)}. \tag{7}$$

The production term $\mathcal{P}$ comes from the first contribution of the sediment flux vector $\mathbf{q}$ (equation (4)) (advective part). According to BEE (equation (5)), it can be approximated by

$$\mathcal{P} \simeq -\overline{hD\,\mathbf{v}\cdot\nabla C} \tag{8}$$

and therefore measures the tendency for growth or decay of bars by the bed flow couplings and bed surf couplings [*Garnier et al.*, 2006]. The damping term Δ comes from the downslope or diffusive contribution of $\mathbf{q}$.

[14] By using the same definition as *Vis-Star et al.* [2008], the "global growth rate" σ of the instability reads

$$\sigma = \frac{1}{\|\,h\,\|^2}\frac{d}{dt}\left(\frac{1}{2}\,\|\,h\,\|^2\right), \tag{9}$$

where $\|h\|$ is the L_2 norm of h and is defined as

$$\|\,h\,\| = \left(\overline{h^2}\right)^{1/2},$$

so that $\|h\|^2$ can be interpreted as the potential energy density of the bed forms [*Vis-Star et al.*, 2008].

[15] To illustrate the physical meaning of σ, let us consider a topographic perturbation like

$$h(x,y,t) = \exp(\sigma_0 t)\,H(x,y), \tag{10}$$

which represents a topographic wave that exponentially grows with a growth rate σ_0 and which keeps a constant shape given by $H(x, y)$, with H being an L_y periodic function with respect to y. This occurs, for instance, during the linear regime (initial stage) of the bar evolution. Then,

$$\sigma(t) = \sigma_0.$$

[16] More generally, the sign of σ determines the different state of the bar evolution: the growth (decay) of the bars can be characterized by $\sigma \gg 0$ ($\sigma < 0$), while the saturation of bars occurs when $\sigma = 0$. Moreover, the global growth rate can be computed with the relationship

$$\sigma = \frac{1}{\|\,h\,\|^2}\,(\mathcal{P} - \Delta), \tag{11}$$

which can be obtained from the definition (equation (9)) by multiplying the BEE (equation (5)) by h and integrating.

3. Model Results

[17] The morphodynamical evolution of an initially alongshore uniform parallel barred beach is studied for hundreds of days. A numerical experimental setup similar to that of *Garnier et al.* [2008] is used. Waves are assumed to arrive normal to the coast. At the offshore boundary

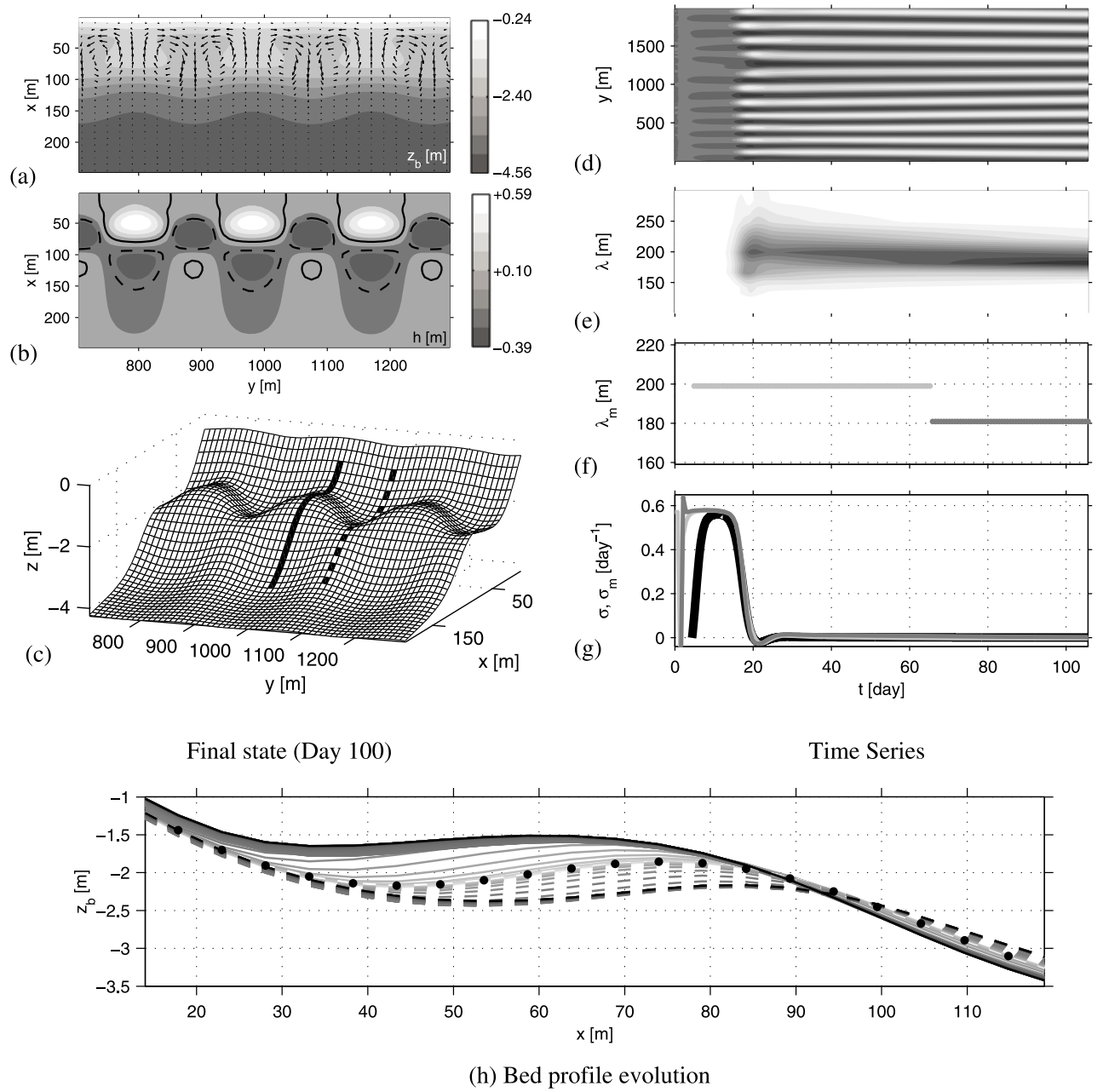

Figure 1. Final state (day 100): (a) top view of the bed level z_b and current vectors **v** and (b) top view of the bed level perturbation h and its contour. Solid (dashed) lines represent the crests (troughs). (c) Tridimensional view of the bed level z_b. Time series: (d) $h(x = 50\text{ m}, y, t)$, bed level perturbation along the longshore section $x = 50$ m (the darker colors represent the deeper areas); (e) $\mathcal{F}(x = 50\text{ m}, \lambda, t)$, its Fourier transform (the darker colors correspond to the more predominant wavelengths); (f) $\lambda_m(x = 50\text{ m}, t)$, resulting predominant wavelength; and (g) growth rates computed with different formula. Black thick line, σ, (global) growth rate computed with relationship (11). Gray thin lines, σ_m, growth rates corresponding to λ_m of Figure 1f. Different gray levels are used to distinguish the two wavelengths. (h) Bed level profile evolution of a crest (solid lines) and of a channel (dashed lines). The selected sections are shown in Figure 1c. The darker the lines are, the longer the evolution is. The dots indicate the initial bed level.

($x = L_x = 250$ m) the height of the incident waves is $H^0_{\text{rms}} = 1$ m, and the period is $T = 6$ s. By perturbing the initial topography, instability develops, and an equilibrium state is eventually reached. The final state is presented in Figures 1a–1c for a random perturbation (perturbation amplitude ~ 1 mm). The evolution of the bed profile is displayed in Figure 1h along a channel and along a crest (as indicated in Figure 1c). It shows that the shore-parallel bar crest, initially at 2 m depth (black dots), subsequently rises up to 1.5 m depth on the crescentic horns (darkest solid line).

[18] Figures 1d–1g show time series of variables taken from the longshore section defined at $x = 50$ m. Figure 1d is

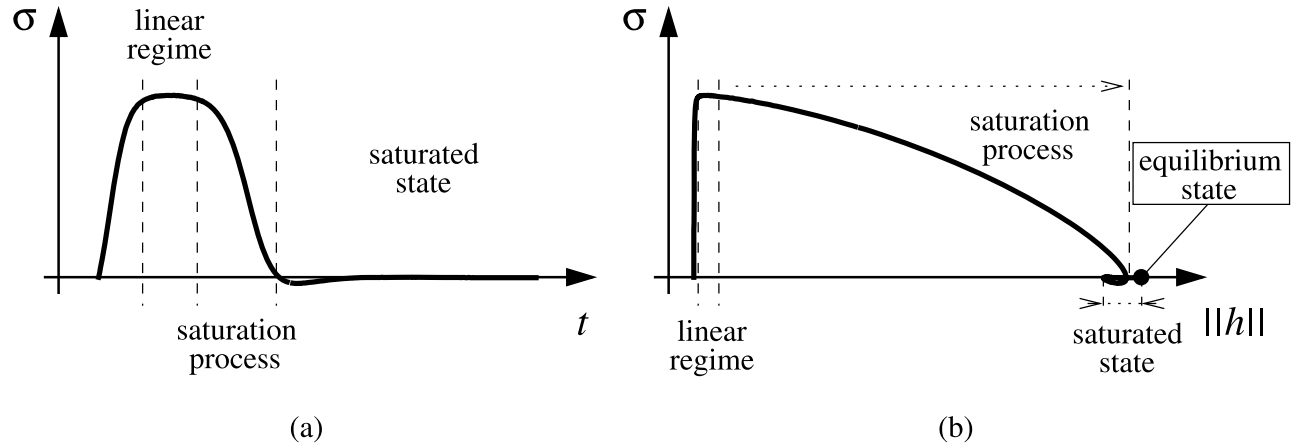

Figure 2. Sketch of the saturation processes: (a) σ as a function of t and (b) σ as a function of $\|h\|$.

the bed level variation, Figure 1e is its Fourier analysis, Figure 1f is the predominant wavelength (λ_m), and in Figure 1g the growth rates (predominant σ_m and global σ) are displayed. The predominant wavelength λ_m (Figure 1f) corresponds to the maximum Fourier coefficient at each time step (plotted in Figure 1e). The growth rate (σ_m) corresponding to λ_m is displayed in Figure 1g. Notice that similar results are obtained if the Fourier analysis is made at another cross-shore location where crescentic bars develop. Thus, these wavelengths correspond to the same unstable mode, that is, the crescentic bar system. At the final state, λ_m = 180 m, and the corresponding initial growth rate (from Fourier analysis) is about $\sigma_m = 0.6\ \mathrm{d}^{-1}$. This growth rate is similar to the initial growth rate corresponding to λ_m = 200 m, which is dominant from day 3 to day 65. Notice that these initial growth rates are taken during the first period where they are constant in time: this period corresponds to the time when the mode amplitude grows exponentially, i.e., to the linear regime. Interestingly, these growth rates obtained from Fourier analysis are similar to the global growth rate σ computed from relationship (11) (Figure 1g, thick black line), which takes into account the overall patterns, not only the features appearing in the section x = 50 m.

[19] The saturation of features begins when σ decreases (Figure 2a). The saturated state is defined as the state for which for the first time $\sigma \simeq 0$. This state can be highly dynamical, in particular if there is merging of bars [*Garnier et al.*, 2006]. The equilibrium state is reached when $\sigma = 0$ for all times. The time taken to reach the equilibrium state is sometimes very long, as the growth rate during the saturated state is small; it can be an order of magnitude longer than the time corresponding to the saturation processes. Because equilibrium is sometimes not observed, its existence is sometimes unknown. Here our interest is the saturation process, so we want to understand why σ decreases. This can be due to either the decrease of the production (more exactly, of $\mathcal{P}/\|h\|^2$) or the increase of the damping term $\Delta/\|h\|^2$.

[20] As Figure 3 shows, there are two ways to observe the evolution of σ and all the variables: as a function of t (Figures 2a and 3a–3e) or of $\|h\|$ (Figure 2b or Figures 3f–3j). The condition of instability is given by $\sigma \gg 0$; that is, the bars grow if $\mathcal{P} \gg \Delta$. It is found that $\mathcal{P}$ and Δ are very similar (Figures 3a and 3f), only their small differences explaining the instability (Figures 3b and 3g).

[21] The difference in the normalized variables $\mathcal{P}/\|h\|^2$ and $\Delta/\|h\|^2$, i.e., σ, should be constant in time for the initial growth of any linearly unstable mode. Because of nonlinearities, it is not constant, and we see that the dynamics of these variables are better represented by analyzing their variations as a function of $\|h\|$ (Figure 3h) rather than time. To be precise, we remark that $\Delta/\|h\|^2$ is constant during the saturation process, while $\mathcal{P}/\|h\|^2$ is only constant at the initial stage, decreasing thereafter until it balances $\Delta/\|h\|^2$.

[22] Thus, the saturation seems to be due to the reduction of the production term rather than an increase of the damping. This will be analyzed in detail in section 4.

4. Physical Mechanisms

4.1. Analysis of the Damping Term

[23] Integrating by parts, and because of the boundary conditions, i.e., because $\alpha(x = 0) \simeq 0$, $h(x = L_x) \simeq 0$, and since h is L_y periodic, we can write

$$\Delta/\ \|\ h\ \|^2 = \frac{\int_0^{L_y}\int_0^{L_x} \Gamma\left\{(\partial_x h)^2 + \left(\partial_y h\right)^2\right\} \mathrm{d}x\ \mathrm{d}y}{\int_0^{L_y}\int_0^{L_x} h^2\ \mathrm{d}x\ \mathrm{d}y} \geq 0\,,$$

so that Δ will contribute to a loss of potential energy [*Vis-Star et al.*, 2008].

4.2. Analysis of the Production Term

4.2.1. Breaking Down the Production

[24] From equation (8), $\mathcal{P}$ can be broken down as $\mathcal{P} = \mathcal{P}_u + \mathcal{P}_v$, with

$$\mathcal{P}_u = -\overline{uh\,D\partial_x C},$$

$$\mathcal{P}_v = -\overline{vh\,D\partial_y C},$$

which describe the role of the cross-shore and the longshore flow components on the production.

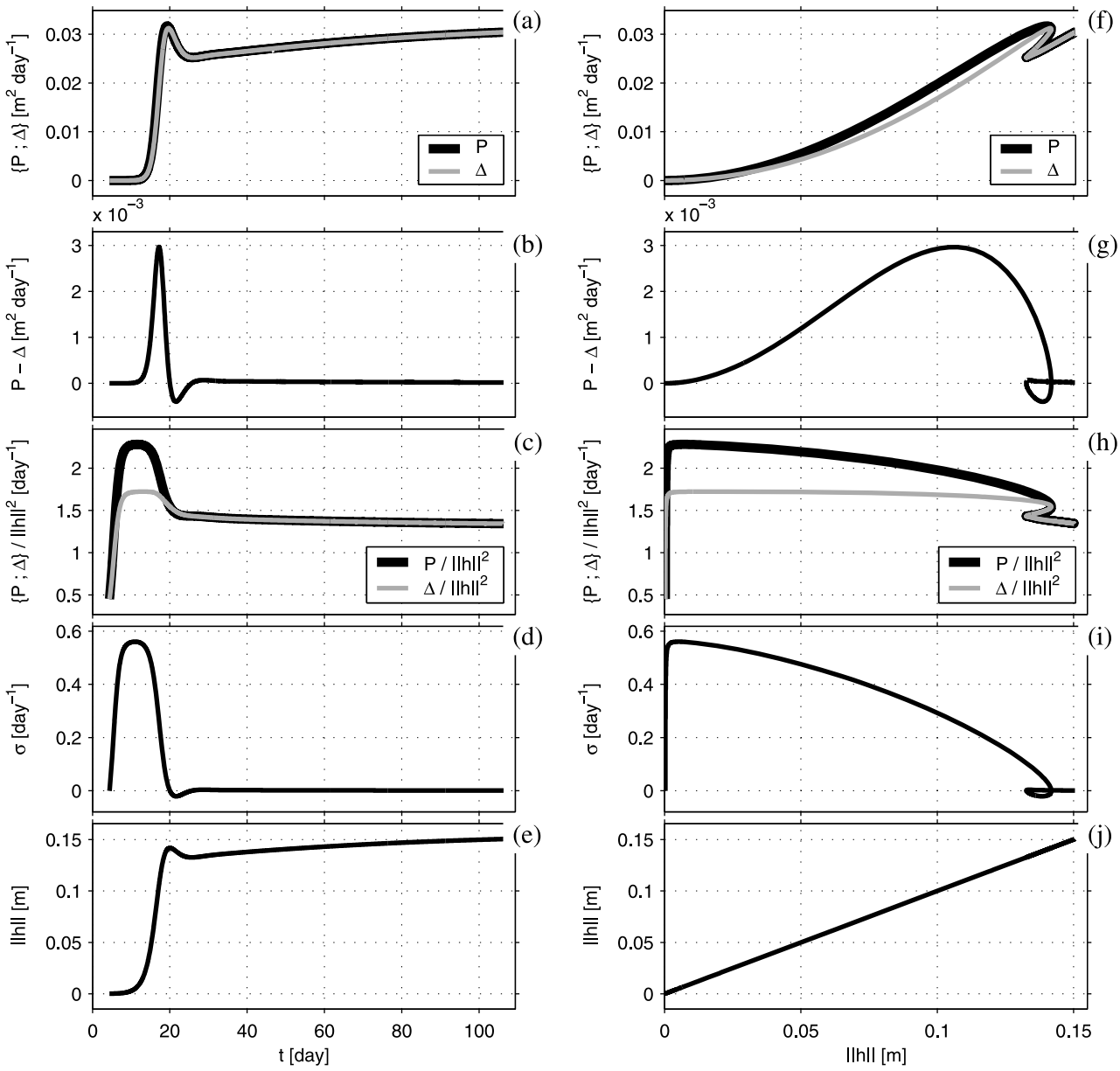

Figure 3. General results obtained from the global analysis. (left) Variables as a function of time. (right) Variables as a function of $\| h \|$. (a, f) Production $\mathcal{P}$ and damping Δ. (b, g) $\mathcal{P} - \Delta$. (c, h) $\mathcal{P}/\|h\|^2$ and $\Delta/\|h\|^2$. (d, i) Global growth rate σ. (e, j) Bar norm $\|h\|$.

[25] Figure 4a shows the $\mathcal{P}_u$ contribution during the saturation process. We see that $\mathcal{P}_u \gg \mathcal{P}_v \geq 0$:

$$\mathcal{P} \simeq \mathcal{P}_u = -\overline{uh\, D\partial_x C}\,. \tag{12}$$

4.2.2. Local Analysis of the Production

[26] The variables controlling the growth and saturation of the bed forms are examined locally by plotting the integrands of (11), (12), and (7) for two different states: during the linear regime (day 11) and during the saturation process (day 19) (Figure 4). In agreement with Figure 3i, the decrease of $\mathcal{P}/\|h\|^2$ (by 26%) with $\|h\|$ is much stronger than the decrease of $\Delta/\|h\|^2$ (by 6%).

[27] To understand the variations of $\mathcal{P}$ and, more particularly, the decrease of $\mathcal{P}/\|h\|^2$ for increasing $\|h\|$, we examine, locally, the variable $uhD\partial_x C$. Figure 5 shows, at the initial state and during the saturation process, the variables $-uh/\|h\|^2$, $D\partial_x C$, and their product $-uhD\partial_x C/\|h\|^2$, which, integrated over the whole domain, gives $\mathcal{P}/\|h\|^2$. From Figures 5a and 5e, the product $-uh$ is seen to be mainly positive, and its highest values are attained where the instability occurs. Where the bars develop, i.e., where the gradient in potential stirring is strong, the variable $D\partial_x C$ is also positive. This explains why $\mathcal{P}$ is positive.

[28] To analyze if the decrease of $\mathcal{P}/\|h\|^2$ is due to a phase shift between $-uh$ and $D\partial_x C$, the correlation between these two signals is examined. The correlation between two real

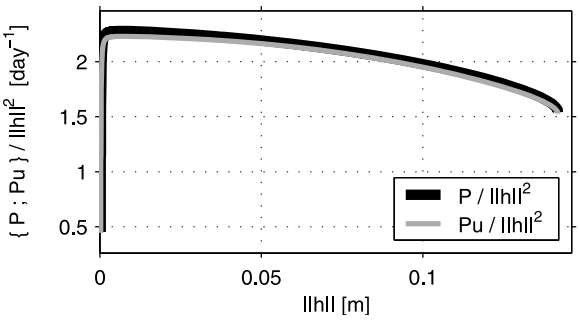

(a) Decomposition of P

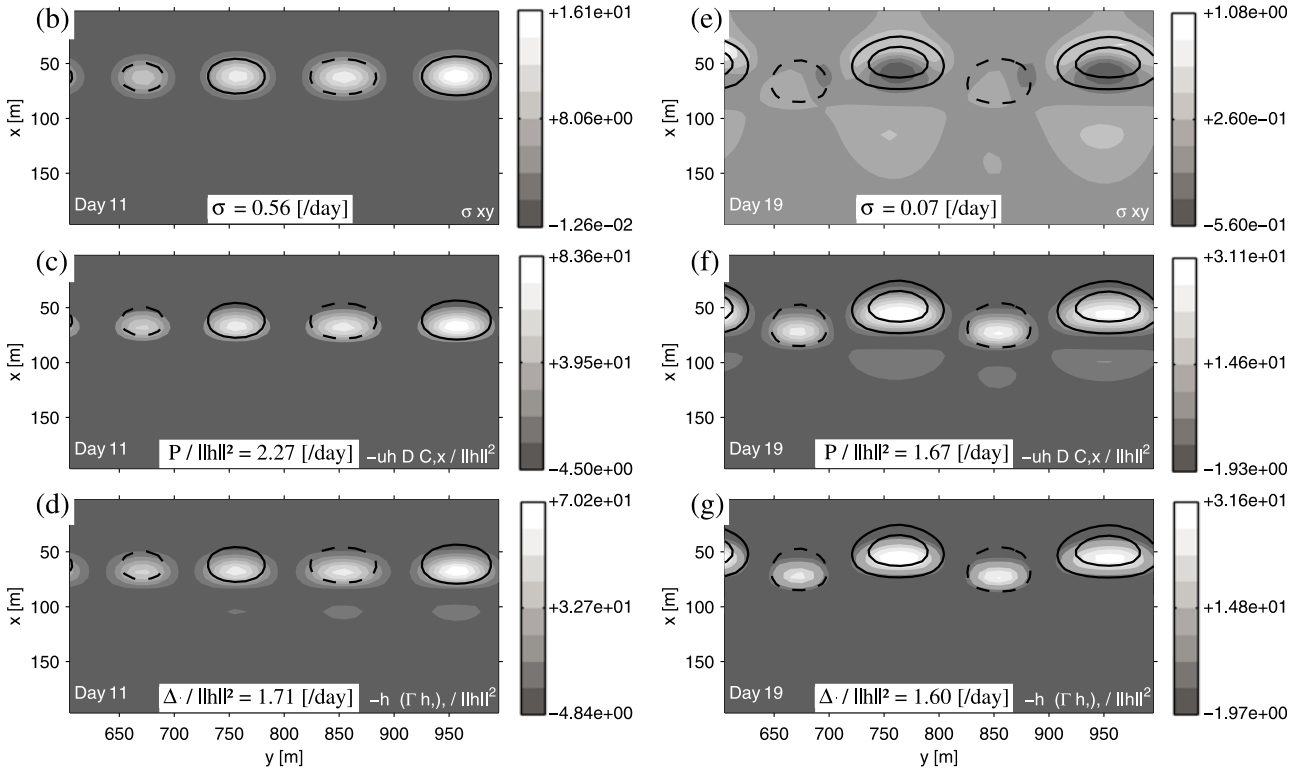

Local analysis

Figure 4. (a) Decomposition of the production $\mathcal{P} \simeq \mathcal{P}_u$: $\mathcal{P}/\|h\|^2$ and $\mathcal{P}_u/\|h\|^2$ as a function of $\|h\|$. (b–g) Local analysis. Contour lines represent the bed level perturbations h; solid (dashed) lines are used for crests (troughs). Figures 4b–4d show the initial state corresponding to the maximum growth rate of instabilities (day 11, linear regime). Figures 4e–4g show the intermediate state corresponding to a decreasing growth rate (day 19, saturation process). Figures 4b and 4e are for $-uhD\partial_x C/\|h\|^2 - h\boldsymbol{\nabla}\cdot(\Gamma\boldsymbol{\nabla}h)/\|h\|^2$. Figures 4c and 4f are for $-uhD\partial_x C/\|h\|^2$. Figures 4d and 4g are for $-h\boldsymbol{\nabla}\cdot(\Gamma\boldsymbol{\nabla}h)/\|h\|^2$.

functions f and g ($f \star g$) is made with a cross correlation defined as

$$f \star g\,(x',y) = \int_0^{L_x} f(x,y)g(x+x',y)\,\mathrm{d}x,$$

where $-L_x < x' < L_x$. For each alongshore location, the cross-shore position of the maximum of $f \star g$, denoted as $x'_\star$, represents the cross-shore shift between f and g. The correlation $-uh/\|h\|^2$ $D\partial_x C$ in Figures 5d and 5h shows that, at the most unstable alongshore location (i.e., over crests or troughs), the cross-shore profiles of the signals $-uh$ and $D\partial_x C$ are centered at the initial state and also during the saturation process. Therefore, the decrease of $\mathcal{P}/\|h\|^2$ is not primarily due, for this specific modeled case, to a shift between the two signals.

[29] Moreover, we notice that the alongshore variations of D and $\partial_x C$ are small compared to those of u and h (Figure 5). Therefore, the effect of the variations in $D\partial_x C$ is negligible in comparison to the effect of the variations of $-uh/\|h\|^2$.

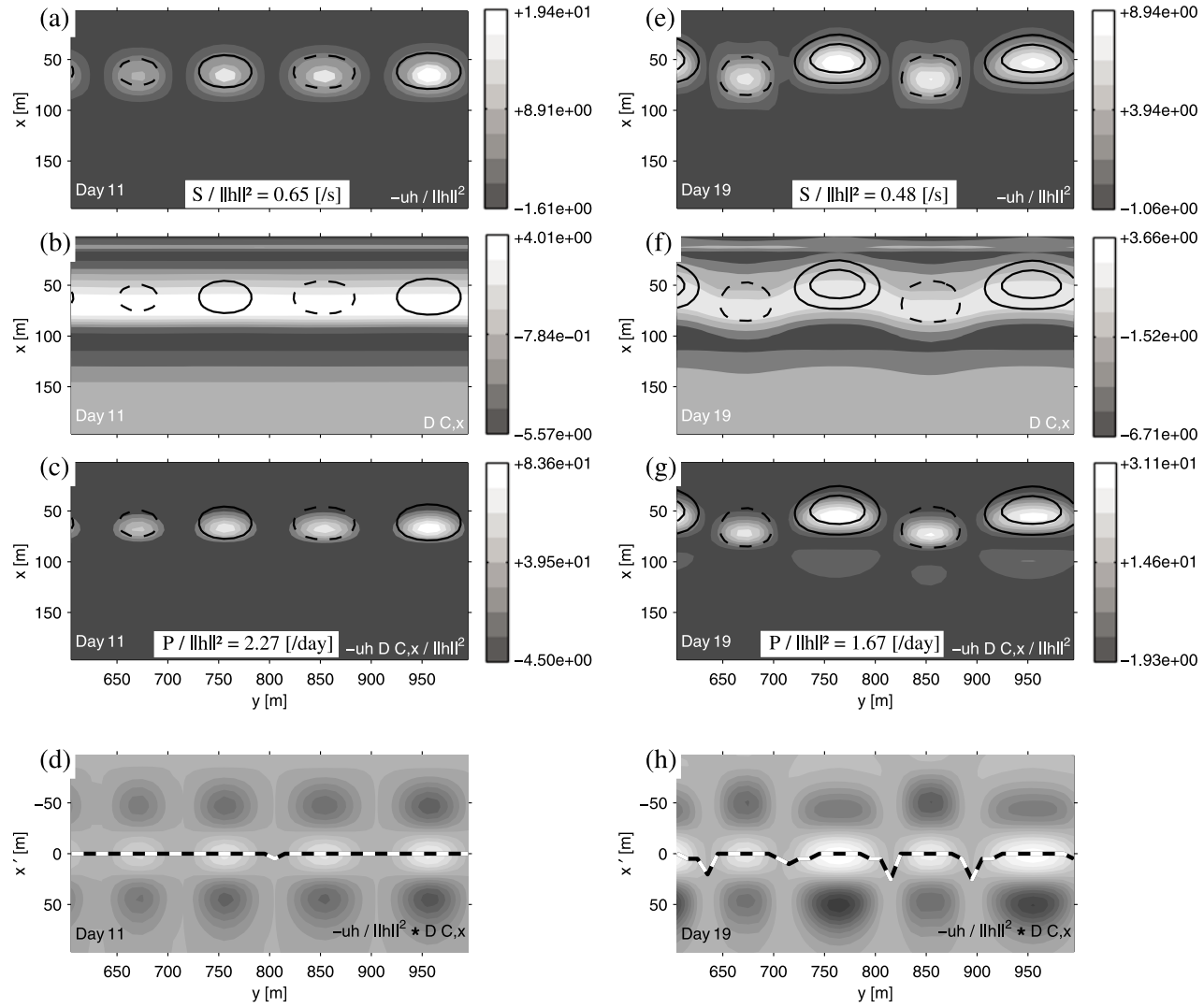

Figure 5. Local analysis of the production. (left) Initial state corresponding to the maximum growth rate of instabilities (day 11, linear regime) and (right) intermediate state corresponding to a decreasing growth rate (day 19, saturation process): (a, e) $-uh/\|h\|^2$, (b, f) $D\partial_x C$, (c, g) $-uhD\partial_x C$, repeated from Figures 4c and 4g (in Figures 5a–5c and 5e–5g, contour lines represent the bed level perturbations h, and solid (dashed) lines are used for crests (troughs)); and (d, h) $-uh/\|h\|^2 \star D\partial_x C$. Small values are shaded, and large values are white. The dashed line defines the maximum for each alongshore location.

[30] In conclusion, the variations of $\mathcal{P}/\|h\|^2$ seem controlled by the local variations of $-uh/\|h\|^2$.

4.2.3. Variations of $-\overline{uh}$

[31] To understand the behavior of $-uh$, we introduce the variable $\mathcal{S}$:

$$\mathcal{S} = -\overline{uh}, \tag{13}$$

which is expected to govern the variation of $\mathcal{P}$. To check this claim, we define S_0 as the average of $\mathcal{P}/\mathcal{S}$ (Figure 6b):

$$S_0 = \frac{\int_0^{\max\|h\|} \mathcal{P}/\mathcal{S}\, \mathrm{d}\, \|h\|}{\max \|h\|}.$$

As shown in Figures 6b and 6c, during the entire saturation process, $\mathcal{P}/\mathcal{S}$ can be approximated as a constant (its relative variation is less than 2%), and

$$\mathcal{P} \simeq S_0\, \mathcal{S}. \tag{14}$$

Thus, $\mathcal{S}$ seems to control the variation of $\mathcal{P}$, and we will focus on investigating why $\mathcal{S}/\|h\|^2$ decreases with $\|h\|$. To understand the variations of the global variable $\mathcal{S}/\|h\|^2$, we can distinguish the processes over the crests and the channels by introducing the variables $\mathcal{S}'_{\mathrm{cha}}$ and $\mathcal{S}'_{\mathrm{bar}}$, which are representative of the quantity $\mathcal{S}/\|h\|^2$ over the channels and the bars, respectively. They read

$$\mathcal{S}'_{\mathrm{cha}} = -\max u/\min h,$$

$$\mathcal{S}'_{\mathrm{bar}} = -\min u/\max h,$$

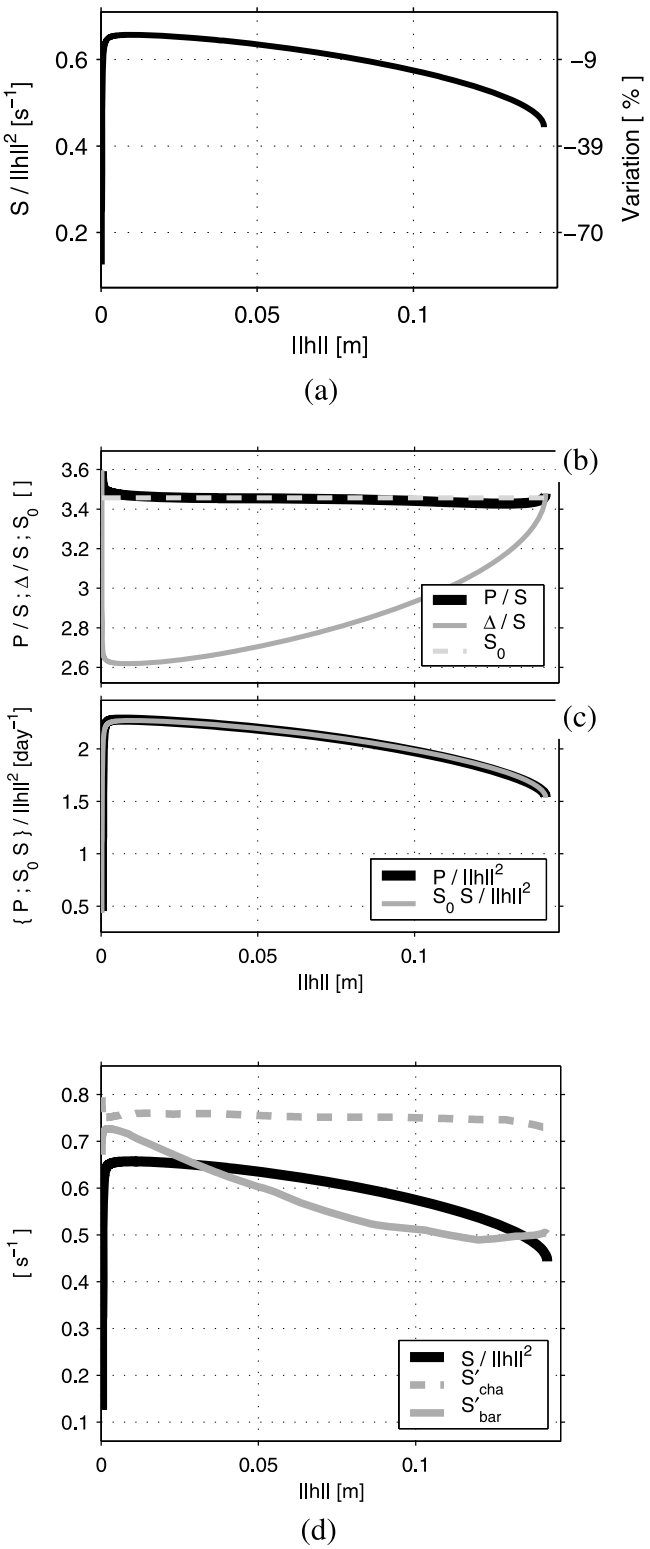

Figure 6. Variations of $-\overline{uh}$. (a) $\mathcal{S}/\|h\|^2$ as a function of $\|h\|$. $\mathcal{P} \simeq S_0\mathcal{S}$: (b) $\mathcal{P}/\mathcal{S}$, $\Delta/\mathcal{S}$, and S_0 as a function of $\| h \|$ and (c) $\mathcal{P}/\| h \|^2$ and $S_0\ \mathcal{S}/\| h \|^2$ as a function of $\|h\|$. (d) $\mathcal{S}/\|h\|^2$ (black solid line), $\mathcal{S}'_{\mathrm{cha}}$ (gray dashed line), and $\mathcal{S}'_{\mathrm{bar}}$ (gray solid line) as a function of $\|h\|$.

where min and max stand for the minimum and maximum value of the variables in the computational domain. Because the current is offshore (onshore) oriented, and h is negative (positive) over a channel (bar), the quantity $\mathcal{S}'_{\mathrm{cha}}$ ($\mathcal{S}'_{\mathrm{bar}}$) is positive. Assuming that in the linear regime $-u$ and h are in phase (and have the same cross-shore distribution), we can write $u(x, y) = -Ah(x, y)$, with $A = \mathcal{S}'_{\mathrm{cha}} = \mathcal{S}'_{\mathrm{bar}} = \mathcal{S}/\|h\|^2$, so that channels and shoals contribute equally. Figure 6d shows that $\mathcal{S}'_{\mathrm{cha}} = \mathcal{S}'_{\mathrm{bar}}$ only at the earliest stage, but later $\mathcal{S}'_{\mathrm{cha}}$ is constant while $\mathcal{S}'_{\mathrm{bar}}$ decreases; thus, the saturation of the crescentic bar growth seems to occur because of the saturation of the bar crests.

4.3. Analysis of the Saturation Process

[32] We have shown that the main reason explaining the saturation of the growth is the decrease of $\mathcal{S}/\|h\|^2$ when the bars grow (reduction by 35%, Figure 6a). This decrease comes from the change in the bar characteristics during the saturation process. The primary bar property that changes during the saturation is the amplitude, and the increase in current intensity with increasing bar amplitude could slow down for large amplitudes. Another possibility for the saturation could be the change in bar shape. In particular, we notice at saturation (Figure 7) that the crests become wider and the channels become narrower, the shoals tend to migrate onshore while the channels migrate offshore, and the deepening of the channels becomes less pronounced than the increased shoal elevation (i.e., the bed level perturbation normalized with the bar norm ($h/\|h\|^2$) increases in the channels when saturation occurs). Actually, these changes in shape properties can be seen as an increase of asymmetry between the linear regime (symmetric bed forms) and the nonlinear stage.

[33] These hypotheses are now investigated by means of "flow over topography" experiments. This means that the model has been used in its hydrodynamical mode (i.e., without sediment transport and bed changes), starting from the same initial profile but superimposing preexisting bed patterns, similar to the rip channel systems obtained by self-organization (Figure 8a). For the default case, the wavelength of the bed forms is set to 200 m, and the amplitude is set to $\max(h) = -\min(h) = 50$ cm, which corresponds to a norm of $\|h\| = 0.11$ m. In each experiment, a hydrodynamical equilibrium state is reached after less than 1 h.

[34] Then the properties of the preexisting bars will be modified to analyze their expected global growth rate if sediment transport and bed evolution were switched on. This fictive growth rate is computed by using formula (11). This allows us to characterize which property of the saturated bar system causes the saturation.

4.3.1. Change in Bar Amplitude

[35] To investigate if the change in bar amplitude affects the growth rate of the instabilities, the amplitude of the imposed features has been varied from 1 mm to 1 m. Figure 8b shows an estimate of the global growth rate σ of these bed forms by using formula (11). Within the range of amplitude simulated in the morphodynamical experiments (i.e., $\|h\| < 0.15$ m), the growth rate decreases with the bar norm, but it does not vanish. Thus, the increase in bar amplitude contributes to the saturation process, but we will see that it is not the main reason. Interestingly, we notice an increase of the growth rate for higher bed forms due to

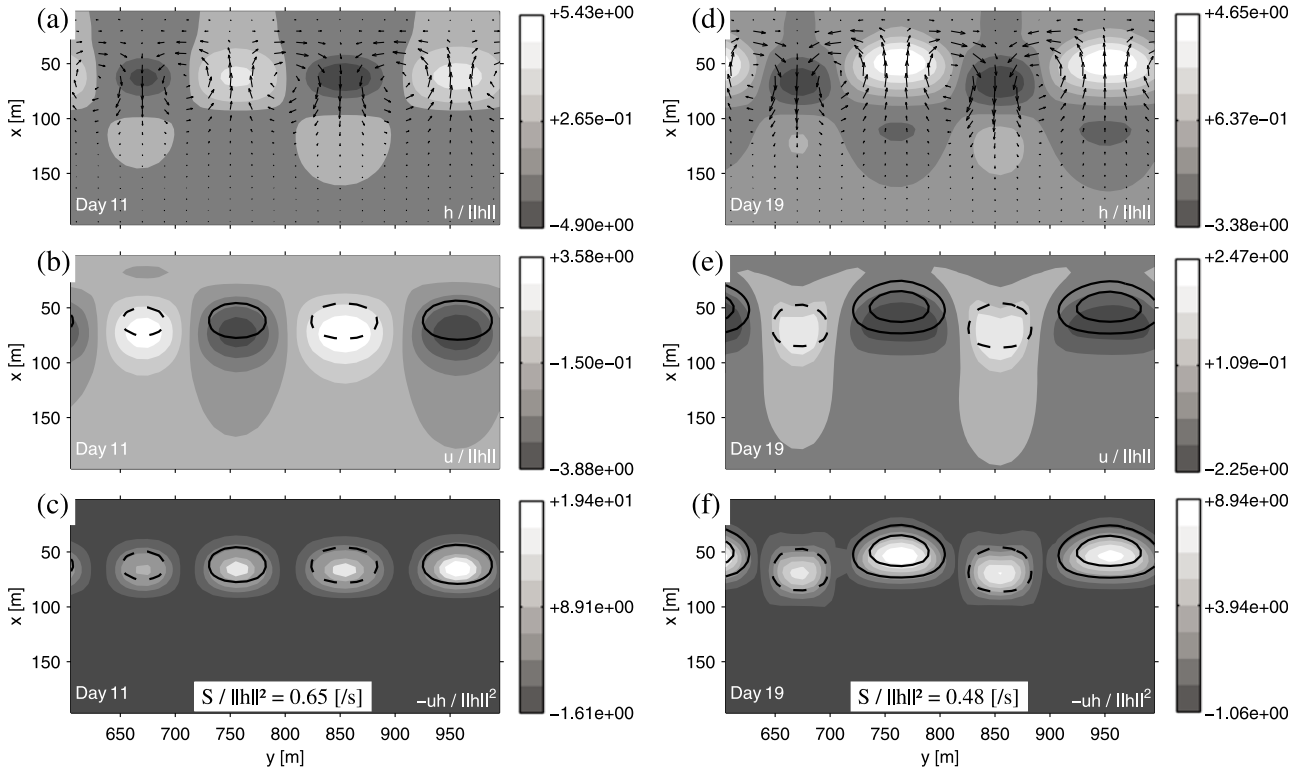

Figure 7. Analysis of the saturation process and change in bar characteristics. (left) Initial state corresponding to the maximum growth rate of instabilities (day 11, linear regime) and (right) intermediate state corresponding to a decreasing growth rate (day 19, saturation process): (a, d) $h/\|h\|$, (b, e) $u/\|h\|$, and (c, f) $-uh/\|h\|^2$, repeated from Figures 5a and 5e. Contour lines represent the bed level perturbations h; solid (dashed) lines are used for crests (troughs).

strong gradients $\partial_x C$, which cause an increase of the production.

4.3.2. Bar Widening

[36] The influence of the bar asymmetry on the cross-shore velocity and on $\mathcal{S}/\|h\|^2$ is investigated here through hydrodynamical experiments. To this end, the alongshore extent of the crests is set to 150 m, and that of the channels is set to 50 m (see contour lines, Figures 9a–9c). We remark that the increase of the asymmetry leads to a reduction in $\mathcal{S}/\|h\|^2$ by 30% in this case (Figures 8d and 9b). This implies that the global growth rate is positive when the bed level is symmetric (Figure 8c), while it is negative with the asymmetry (Figure 9a). A comparison between Figures 8d and 9b shows that $\mathcal{S}'_{\text{bar}}$ decreases because the onshore current magnitude over the larger crest decreases (Figures 8e and 9c). However, there is not clear reduction of $\mathcal{S}'_{\text{cha}}$ as the offshore current is stronger in the narrow channel (Figures 8e and 9c), in agreement with Figure 6d. Actually, $\mathcal{S}/\|h\|^2$ globally decreases because the bar widening implies that the crests hold relatively more space than the channels.

4.3.3. Onshore Bar Migration

[37] The analysis of the growth rate, locally (Figure 8c), shows that the initial bed forms that were aligned on the same alongshore axis tend to migrate cross-shore, the crests (channels) migrating onshore (offshore), as it is observed in the self-organized patterns. This characteristic of rip channel systems is also a reason for the growth saturation. By including an onshore (offshore) shift of the bars (channels) of 20 m, Figures 9d–9f show that the topography is less prone to instability and that the bed forms tend to be damped (Figure 9d). As with the introduction of asymmetry, the growth rate is found to be negative because of a strong decrease of onshore flow over the bar. The magnitude of the offshore flow is slightly increased, but we notice a global weaker current circulation that results in a decrease of $\mathcal{S}/\|h\|^2$.

4.3.4. Change in Mean Beach Profile

[38] During the evolution, the beach profile changes (Figure 10) as the crests migrate onshore and the channels migrate offshore. Thus, there is a global (slight) onshore migration of the longshore bar. Moreover, the mean beach profile is affected by a bed rise in the crests relatively stronger than a bed fall in the channels (compare maximum and minimum values in Figure 10b), so that $h/\|h\|$ increases in the channels and remains almost constant at the crests (Figure 10c). This could be because of a higher downslope transport in the channels than on the crests due to stronger gradients induced by the asymmetry. This increase of $h/\|h\|$ causes a decrease of production in the channel and also a weaker current circulation in the whole domain and therefore a reduction of the global production.

4.3.5. Comparison With Observations

[39] The fundamental interest of the finite amplitude modeling is revealed when comparing model results with field observations, as real bars are finite amplitude features. Interestingly, despite the simplicity of the model, the bar

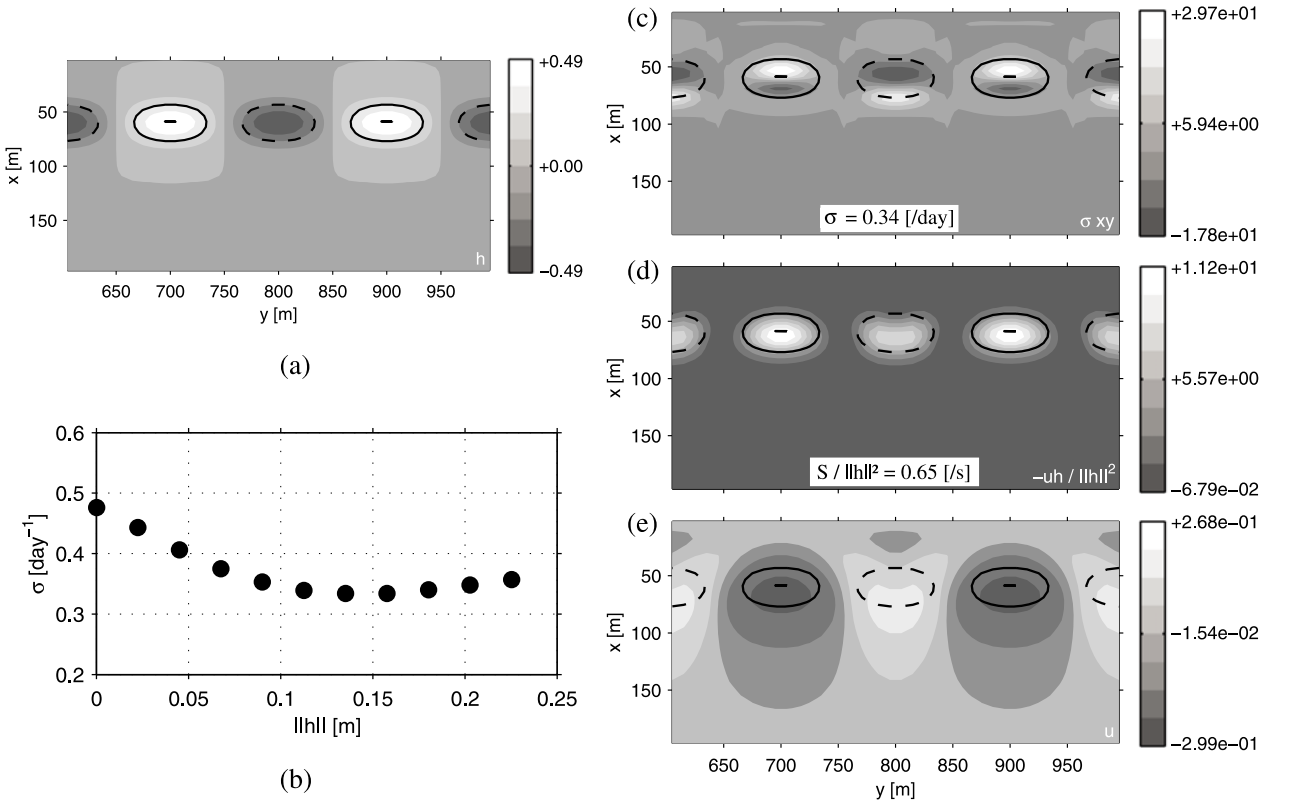

Figure 8. Change in bar amplitude. Hydrodynamical experiments. (a) Linear bed level perturbation for an amplitude of max(h) = 50 cm ($\| h \|$ = 0.11 m) and (b) σ as a function of the bar norm $\|h\|$ at the hydrodynamical equilibrium state. Equilibrium state (max(h) = 50 cm): (c) $-uhD\partial_x C/\|h\|^2 - h\nabla \cdot (\Gamma \nabla h)/\|h\|^2$, (d) $-uh/\|h\|^2$, and (e) u. Contour lines represent the bed level perturbations h; solid (dashed) lines are used for crests (troughs).

shape at the final state that causes the saturation seems to be consistent with the observations of mature crescentic bar systems.

[40] First, the commonly observed narrow jet-like rip currents along with wider and weaker onshore return currents [*Short*, 1999; *MacMahan et al.*, 2006] are reproduced here as a result of nonlinearity (the alongshore profiles being sinusoidal for the linear regime). In our morphodynamical model, which couples morphology and circulation, the widths of the rips and of the return currents are correlated with the widths of the channels and shoals, respectively. The rip currents being narrower than the return currents is a very robust characteristic of the system, and it has been shown to occur even in the absence of bed changes because of conservation of vorticity for a horizontal circulation (purely hydrodynamical problem) on a plane sloping beach [*Arthur*, 1962]. In this case, if rip channels are just carved by the current, their widths should be correlated too. This correlation between narrow rips and narrow channels is also observed in some intertidal bars [*Castelle et al.*, 2007; *Bruneau et al.*, 2009]. Therefore, all this suggests that the narrowing of the channels and widening of the shoals that has been shown to slow down the growth of the crescentic pattern would be characteristic of mature crescentic bars. However, from bathymetric measurements there is no general evidence for the narrowing of the channels. Moreover, experimental studies do not show the correlation between the width of the narrow rip currents and the width of the channels. This could be due to the difficulties in getting current measurements and underlying bathymetry in the surf zone. For instance, during the Rip Current Experiment (RIPEX) [*MacMahan et al.*, 2005, 2006], for some particular events, the channels can appear wider than the bars. But the data are given for a fixed cross-shore location without taking into account the cross-shore variability. This could be critical because the widths of the channels and of the bars should be measured where the bed alongshore variability is the highest or where the cross-shore current magnitude is the strongest. Therefore, in the absence of systematic bathymetric measurements, we conclude that the widely observed asymmetry in the circulation indicates that although there is no clear direct experimental evidence of the corresponding asymmetry between channels and shoals, it is, in general, very likely to occur.

[41] Second, the onshore (offshore) migration of the crests (channels) can be seen as a step in the transition "Rhythmic Bar and Beach" to "Transverse Bar and Rip" of the *Short* [1999] classification [*Ranasinghe et al.*, 2004; *Garnier et al.*, 2008]. This transition typically occurs for calm wave conditions following a storm, which is consistent with the presented simulations. Moreover, this behavior of the crescentic bar system is linked to an onshore migration of the mean parallel bar, due to a net sand deposition shoreward of the bar and erosion seaward.

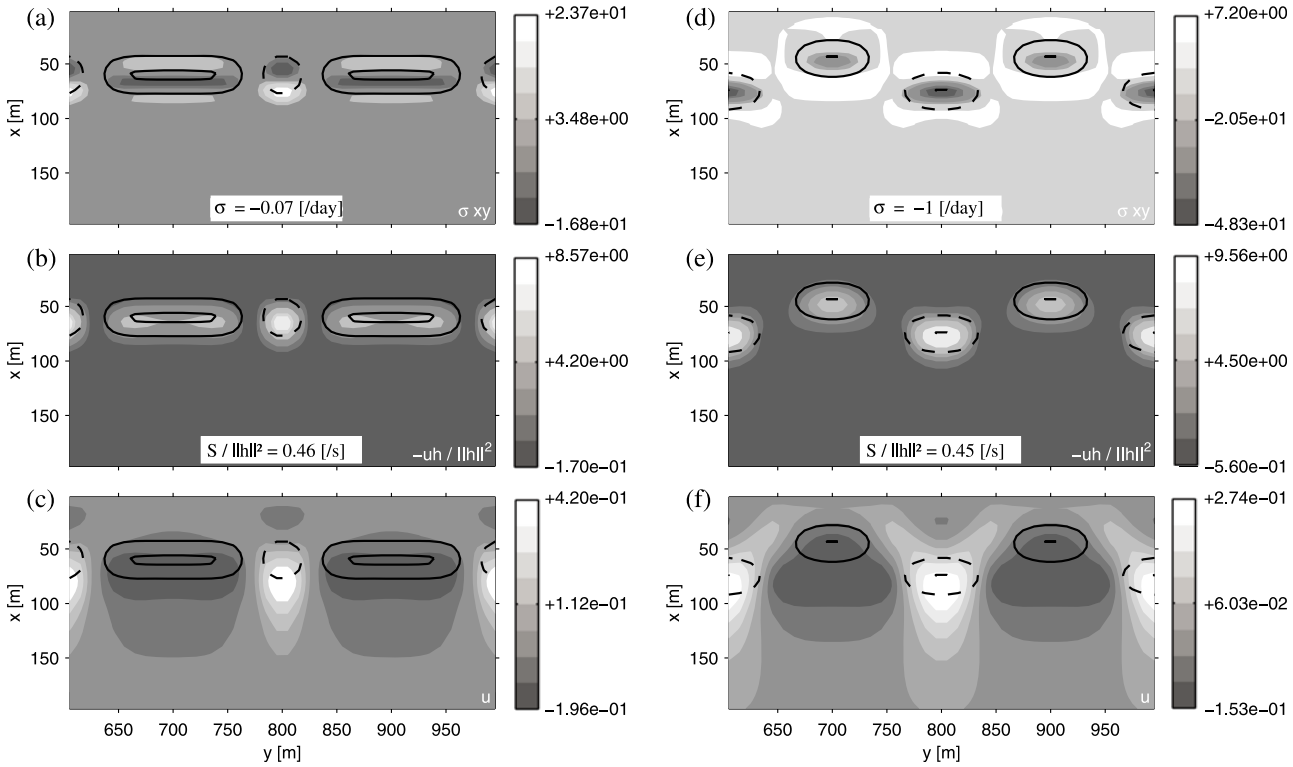

Figure 9. Change in bar shape. Hydrodynamical experiments. (left) Bars and channels, alongshore extended and reduced, respectively, by 50 m and (right) bars and channels, onshore and offshore shifted, respectively, by 20 m: (a, d) $-uhD\partial_x C/\|h\|^2 - h\nabla \cdot (\Gamma \nabla h)/\| h \|^2$, (b, e) $-uh/\| h \|^2$, and (c, f) u. Contour lines represent the bed level perturbations h; solid (dashed) lines are used for crests (troughs).

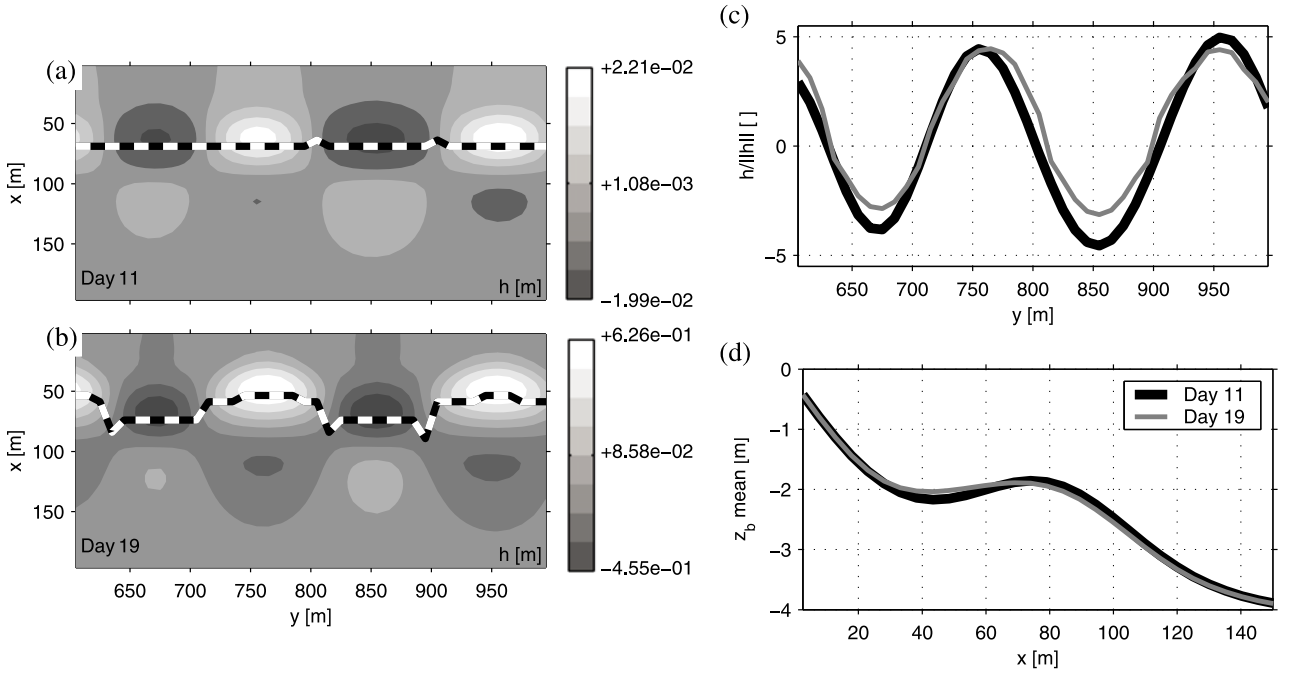

Figure 10. Change in mean beach profile. Bed perturbation h, the dashed line indicates the cross-shore position of the maximum production for each alongshore location: (a) initial state (day 11) and (b) intermediate state (day 19). (c) Alongshore profiles of $h/\|h\|$ following the dashed line of Figures 10a and 10b. (d) Cross-shore profiles of $z_{b_{\text{mean}}}(x) = \text{mean}_y(z_b(x, y))$. The thick black line corresponds to the beginning of the evolution (Figure 10a), and the thin gray line corresponds to the saturation process (Figure 10b).

[42] Interestingly, this global migration is exclusively due to 2-D circulations as the cross-shore sediment transport processes (undertow, wave asymmetry, etc.) are assumed to be in balance. This result is in agreement with the empirical modeling study of *Plant et al.* [2006], as it illustrates the coupling between the bathymetric alongshore variability and the displacement of the shore-parallel bar. The alongshore variability, which can be seen as the cross-shore span of the crescentic system (as defined by *Plant et al.* [2006]), becomes stronger because of the increase of the bar amplitude, the onshore migration of the crests, and the offshore migration of the channels (although the increase of the bar amplitude induces the migrations by producing the nonlinearities). This will cause the net onshore bar migration. Moreover, in this particular experiment, which is representative of calm, stationary wave conditions approaching a beach previously smoothed by a storm, a morphodynamical equilibrium state is obtained, and it is characterized by an increase of the variability and by the onshore migration of the parallel bar, as *Plant et al.* [2006] suggests.

[43] More generally, the overall changes in bar shape causing the growth saturation (the bar widening, the onshore crest migration, and the decreasing channel depth) comprise a development of bar asymmetry due to the nonlinearity of the beach system. All of them lead to a change in the mean beach profile. This shows the importance of the role of the alongshore variability and of the 2-D nonlinear processes in the cross-shore dynamics, which are generally not addressed by 1-D cross-shore modeling studies.

5. Conclusions

[44] The reasons for the saturation of the growth of crescentic bars emerging from self-organization of an initially straight parallel bar have been investigated for normal wave incidence. The saturation process is defined as the transition between the linear regime (maximum and constant growth rate) and the saturated state (negligible growth). A wave- and depth-averaged nonlinear shallow water equation solver with wave transformation, sediment transport, and bed updating has been used to reproduce the saturation and therefore to simulate the finite amplitude behavior of such rhythmic systems. Thereafter, the global analysis of the beach system has been used to understand the mechanisms behind the saturation process. It consists of studying the global properties of the morphodynamical patterns over the whole computational domain. In particular, the potential energy balance of the morphological pattern gives an expression for the growth rate as the difference between the production (related to the positive feedback leading to the instability) and the damping (loss of energy due to the gravity-driven downslope transport). To understand which aspects of the developing bar system cause the decrease of the growth rate, a new method is introduced. It is based on computing the hydrodynamics on preexisting fixed (i.e., no sediment transport) arbitrary morphological patterns (called the "flow over topography" problem). This has been used in previous studies in the case of a local morphodynamical analysis, but the innovative aspect here is its combination with the global analysis, which allows us to compute the fictive growth rate of the patterns, along with the production and damping terms.

[45] The analysis leads to the following conclusions. (1) Although the damping is essential for the onset of the saturation, it is remarkable that the saturation occurs because of a weakening of the instability mechanism rather than an increase of the damping. (2) The effect of the alongshore component of the current in the bar evolution is negligible during both the initial development and the saturation process. (3) The saturation of the crescentic patterns is substantially due to the changes in bar shape from its initial stage rather than the growth in amplitude itself. (4) The alongshore variability of the topography induces the displacement of the mean shore-parallel bar.

[46] Although the conclusions are drawn for a specific modeled case, the method introduced here is likely to be applicable to other types of sandbars.

[47] **Acknowledgments.** The work of R. Garnier was supported by the University of Nottingham and is part of the Spanish Government project under contract CTM2006-08875. Their support is gratefully acknowledged. We thank Paolo Blondeaux, the anonymous reviewer, and the associate editor for their useful reviews.

References

Arthur, R. (1962), A note on the dynamics of rip currents, *J. Geophys. Res.*, *67*, 2777–2779.

Bowen, A. J., and D. L. Inman (1971), Edge waves and crescentic bars, *J. Geophys. Res.*, *76*, 8662–8671.

Bruneau, N., et al. (2009), Field observations of an evolving rip current on a meso-macrotidal well-developed inner bar and rip morphology, *Cont. Shelf Res.*, *29*, 1650–1662.

Caballeria, M., G. Coco, A. Falqués, and D. A. Huntley (2002), Self-organization mechanisms for the formation of nearshore crescentic and transverse sand bars, *J. Fluid Mech.*, *465*, 379–410.

Calvete, D., and H. E. de Swart (2003), A nonlinear model study on the long-term behavior of shore face-connected sand ridges, *J. Geophys. Res.*, *108*(C5), 3169, doi:10.1029/2001JC001091.

Calvete, D., N. Dodd, A. Falqués, and S. M. van Leeuwen (2005), Morphological development of rip channel systems: Normal and near normal wave incidence, *J. Geophys. Res.*, *110*, C10006, doi:10.1029/2004JC002803.

Calvete, D., G. Coco, A. Falqués, and N. Dodd (2007), (Un)predictability in rip channel systems, *Geophys. Res. Lett.*, *34*, L05605, doi:10.1029/2006GL028162.

Castelle, B., P. Bonneton, H. Dupuis, and N. Senechal (2007), Double bar beach dynamics on the high-energy meso-macrotidal French Aquitanian coast: A review, *Mar. Geol.*, *245*, 141–159.

Damgaard, J., N. Dodd, L. Hall, and T. Chesher (2002), Morphodynamic modelling of rip channel growth, *Coastal Eng.*, *45*, 199–221.

Deigaard, R., N. Drnen, J. Fredsoe, J. H. Jensen, and M. P. Jrgesen (1999), A morphological stability analysis for a long straight barred coast, *Coastal Eng.*, *36*, 171–195.

Dronen, N., and R. Deigaard (2007), Quasi-three-dimensional modelling of the morphology of longshore bars, *Coastal. Eng.*, *54*, 197–215.

Falqués, A., G. Coco, and D. A. Huntley (2000), A mechanism for the generation of wave-driven rhythmic patterns in the surf zone, *J. Geophys. Res.*, *105*, 24,071–24,088.

Garnier, R., D. Calvete, A. Falqués, and M. Caballeria (2006), Generation and nonlinear evolution of shore-oblique/transverse sand bars, *J. Fluid Mech.*, *567*, 327–360.

Garnier, R., D. Calvete, A. Falqués, and N. Dodd (2008), Modelling the formation and the long-term behavior of rip channel systems from the deformation of a longshore bar, *J. Geophys. Res.*, *113*, C07053, doi:10.1029/2007JC004632.

Holman, R. A., and A. J. Bowen (1982), Bars, bumps, and holes: Models for the generation of complex beach topography, *J. Geophys. Res.*, *87*, 457–468.

Klein, M. D., and H. M. Schuttelaars (2006), Morphodynamic evolution of double-barred beaches, *J. Geophys. Res.*, *110*, C06017, doi:10.1029/2005JC003155.

Lafon, V., D. D. M. Apoluceno, H. Dupuis, D. Michel, H. Howa, and J. M. Froidefond (2004), Morphodynamics of nearshore rhythmic sandbars in a mixed-energy environment (SW France): I. Mapping beach changes using visible satellite imagery, *Estuarine Coastal Shelf Sci.*, *61*, 289–299.

MacMahan, J. H., E. B. Thornton, T. P. Stanton, and A. J. H. M. Reniers (2005), RIPEX: Observations of a rip current system, *Mar. Geol.*, *218*, 113–134.

MacMahan, J. H., E. B. Thornton, and A. J. H. M. Reniers (2006), Rip current review, *Coastal Eng.*, *53*, 191–208.

Marieu, V., P. Bonneton, D. Foster, and F. Ardhuin (2008), Modeling of vortex ripple morphodynamics, *J. Geophys. Res.*, *113*, C09007, doi:10.1029/2007JC004659.

Mei, C. C. (1989), *The Applied Dynamics of Ocean Surface Waves*, *Adv. Ser. Ocean Eng.*, vol. 1, World Sci., Singapore.

Plant, N. G., K. T. Holland, and R. A. Holman (2006), A dynamical attractor governs beach response to storms, *Geophys. Res. Lett.*, *33*, L17607, doi:10.1029/2006GL027105.

Ranasinghe, R., G. Symonds, K. Black, and R. Holman (2004), Morphodynamics of intermediate beaches: A video imaging and numerical modelling study, *Coastal Eng.*, *51*, 629–655.

Reniers, A. J. H. M., J. A. Roelvink, and E. B. Thornton (2004), Morphodynamic modeling of an embayed beach under wave group forcing, *J. Geophys. Res.*, *109*, C01030, doi:10.1029/2002JC001586.

Ribas, F., A. Falqués, and A. Montoto (2003), Nearshore oblique sand bars, *J. Geophys. Res.*, *108*(C4), 3119, doi:10.1029/2001JC000985.

Roos, P. C., S. J. M. Hulscher, M. A. F. Knaapen, and R. M. J. V. Damme (2004), The cross-sectional shape of tidal sandbanks: Modeling and observations, *J. Geophys. Res.*, *109*, F02003, doi:10.1029/2003JF000070.

Ruessink, B. G., G. Coco, R. Ranasinghe, and I. L. Turner (2007), Coupled and noncoupled behavior of three-dimensional morphological patterns in a double sandbar system, *J. Geophys. Res.*, *112*, C07002, doi:10.1029/2006JC003799.

Short, A. D. (1999), *Handbook of Beach and Shoreface Morphodynamics*, John Wiley, New York.

Smit, M., A. Reniers, B. Ruessink, and J. Roelvink (2008), The morphological response of a nearshore double sandbar system to constant wave forcing, *Coastal Eng.*, *55*, 761–770.

Soulsby, R. L. (1997), *Dynamics of Marine Sands*, Thomas Telford, London.

van Enckevort, I. M. J., B. G. Ruessink, G. Coco, K. Suzuki, I. L. Turner, N. G. Plant, and R. A. Holman (2004), Observations of nearshore crescentic sandbars, *J. Geophys. Res.*, *109*, C06028, doi:10.1029/2003JC002214.

van Leeuwen, S. M., N. Dodd, D. Calvete, and A. Falqués (2006), Physics of nearshore bed pattern formation under regular or random waves, *J. Geophys. Res.*, *111*, F01023, doi:10.1029/2005JF000360.

Vis-Star, N., H. de Swart, and D. Calvete (2008), Patch behaviour and predictability properties of modelled finite-amplitude sand ridges on the inner shelf, *Nonlinear Processes Geophys.*, *15*, 943–955.

Wright, L. D., and A. D. Short (1984), Morphodynamic variability of surf zones and beaches: A synthesis, *Mar. Geol.*, *56*, 93–118.

D. Calvete, A. Falqués, and R. Garnier, Departament de Física Aplicada, Universitat Politécnica de Catalunya, Campus Nord, Modùl B4, E-08034 Barcelona, Spain. (calvete@fa.upc.edu; falques@fa.upc.edu; roland.garnier@gmail.com)

N. Dodd, Environmental Fluid Mechanics Research Centre, Process and Environmental Division, Faculty of Engineering, University of Nottingham, University Park, Nottingham NG7 2RD, UK. (nick.dodd@nottingham.ac.uk)